

## Article

# Preparation of $\text{CuCrO}_2$ Anisotropic Dela-fossite-Type Thin Film by Electrospinning on Glass Substrates

Chung-Lun Yu <sup>1</sup>, Chia-Hsuan Weng <sup>1</sup>, Rong-Jun Huang <sup>1</sup>, Subramanian Sakthinathan <sup>1</sup>, Te-Wei Chiu <sup>1,\*</sup>   
and Chaofang Dong <sup>2,\*</sup>

- <sup>1</sup> Department of Materials and Mineral Resources Engineering, National Taipei University of Technology, 1, Section 3, Zhongxiao E. Road, Taipei 106, Taiwan; samweo909li@gmail.com (C.-L.Y.); a0919861827@gmail.com (C.-H.W.); bruce811018@gmail.com (R.-J.H.); sakthinathan@ntut.edu.tw (S.S.)
- <sup>2</sup> Corrosion and Protection Center, Key Laboratory for Corrosion and Protection (MOE), University of Science and Technology Beijing, No. 30 Xueyuan Road, Beijing 100083, China
- \* Correspondence: tewei@ntut.edu.tw (T.-W.C.); cfdong@ustb.edu.cn (C.D.);  
Tel.: +886-2-2771-2171#2742 (T.-W.C.); +86-106-233-3931 (C.D.)

**Abstract:** Anisotropic  $\text{CuCrO}_2$  thin films were successfully prepared on glass substrate by the electrospinning method followed by annealing at 600 °C. The directionality of the nanowires increased with increases in rotation speed. In addition, the structural formation and optoelectronic behavior of the  $\text{CuCrO}_2$  thin films have been studied by X-ray powder diffraction studies, transmission electron microscopy, field emission scanning electron microscopy, and UV-vis spectroscopy. The X-ray diffraction studies revealed a delafossite properties of the  $\text{CuCrO}_2$ . The electrical conductivity in the parallel and vertical directions of the films produced at 2000–3000 rpm differed by two to three orders of magnitude. The optical transmittance properties of the  $\text{CuCrO}_2$  thin films were improved by increasing the rotation speed.

**Keywords:**  $\text{CuCrO}_2$ ; thin film; anisotropic; electrospinning; electrical conductivity; optical properties



**Citation:** Yu, C.-L.; Weng, C.-H.; Huang, R.-J.; Sakthinathan, S.; Chiu, T.-W.; Dong, C. Preparation of  $\text{CuCrO}_2$  Anisotropic Dela-fossite -Type Thin Film by Electrospinning on Glass Substrates. *Ceramics* **2021**, *4*, 364–377. <https://doi.org/10.3390/ceramics4030026>

Academic Editors: Anna Lukowiak and Gilbert Fantozzi

Received: 9 April 2021  
Accepted: 20 June 2021  
Published: 22 June 2021

**Publisher's Note:** MDPI stays neutral with regard to jurisdictional claims in published maps and institutional affiliations.



**Copyright:** © 2021 by the authors. Licensee MDPI, Basel, Switzerland. This article is an open access article distributed under the terms and conditions of the Creative Commons Attribution (CC BY) license (<https://creativecommons.org/licenses/by/4.0/>).

## 1. Introduction

Metal oxides are a class of materials with a wide range of characteristics that are becoming increasingly used in a variety of applications. Moreover, metal oxides have a high heat of formation and a huge band gap due to the strong metal–oxygen bond [1,2]. Transparent conducting oxides (TCO) are special semiconductors combining electrical conductivity and visible-range transparency in a single material [3]. They are used in a wide range of optoelectronic applications, such as photovoltaic cells, solar cells, flat panel displays, and gas sensors, and light-emitting diodes [4–7]. The popular TCOs currently used are n-type, of which In-doped  $\text{SnO}_2$  and F-doped  $\text{SnO}_2$  dominate the market for unique properties [8]. However, improvements to modern optoelectronic devices are based on p–n junctions, so the development of p-type materials is important. At present, p-type TCOs are generally less evolved and less used than n-type TCOs. The  $\text{CuAlO}_2$  was first described in 1997 for a highly conductive p-type TCO material [9]. A series of p-type TCOs based on Cu-incorporating oxides, such as  $\text{CuCrO}_2$  [10],  $\text{CuFeO}_2$  [11],  $\text{CuInO}_2$  [12],  $\text{SrCu}_2\text{O}_2$  [13],  $\text{CuScO}_2$ , and  $\text{CuGaO}_2$  [14] have been established as a result of material discovery efforts following the principle. Hence, the improvement of p-type TCO materials is a worthy endeavor.

The  $\text{CuCrO}_2$  is p-type TCO [15,16], which can be prepared by different techniques, such as chemical vapor deposition (CVD) [17], pulsed laser deposition [18–21], sol-gel techniques [22,23], hydrothermal synthesis [24], electron beam evaporation [25], sputtering [26–28] and so on. However, electrospinning is more interesting because it is conducted at room temperature [29]. It is also a simple technique for nanowire preparation [30]. There are three key components of an electrospinning system: a high voltage power unit,

a spinneret, and a collecting plate. A voltage is applied to the metal source to inject a charge of a certain polarity into a loaded polymer solution, which is then expelled into an opposite polarity collector [31,32]. A polymer gel solution retained by its surface tension at the end of a tube is subjected to an electric field in the electrospinning. A charge is caused by the applied electric field on the liquid top surface. Repulsive electrostatic charge produces a force that is directly opposite to the surface tension of the polymer. The repulsive electrical force surpasses the surface tension force when the applied electric field exceeds a critical value [33]. Eventually, from the tip of the tube, the charged polymer solution is expelled, forming a Taylor cone and becoming unstable. As a result, the jet is easily whipped between the capillary tip and the collector, resulting in solvent evaporation [34,35]. In this article, we describe the preparation of  $\text{CuCrO}_2$  films by a simple electrospinning method and investigations of the prepared  $\text{CuCrO}_2$  films to determine their morphological structures, electrical, and optical properties. The results indicated that the rotation speed and temperature influence the morphological structure of  $\text{CuCrO}_2$  nanowires.

## 2. Materials and Methods

### 2.1. Instrumentation

Copper nitrate ( $\text{Cu}(\text{NO}_3)_2$ ) and chromium (II) acetate were purchased from Aldrich and AVATOR. Ethanol and polyvinyl pyrrolidone (PVP) were purchased from Echo Chemical Co., Ltd. A study of field emission scanning electron microscopy (FE-SEM) was performed with a Hitachi S-470000. The material structure was identified with a JEOL 2100F transmission electron microscope (TEM). The elemental analysis (EDX) was performed with a HORIBA EMAX-ACT (model 51-ADD0009). The crystal structures were characterized with a GA-XRD PANalytical X'pert X-ray diffractometer (XRD). The optical transmission spectra were measured with a Shimadzu UV-2600 model spectrometer at a range of 200–1100 nm. The electrical conductance of the nanowires was measured with KEITHLEY 2634B two-point probe method at room temperature. To measure the electrical conductance, Al-doped ZnO (AZO) thin films were deposited by RF magnetron sputtering via scotch tape as a mask to form two contact electrodes, as shown in Figure 12.

### 2.2. $\text{CuCrO}_2$ Thin Film Preparation

The  $\text{CuCrO}_2$  nanowire was prepared by a simple electrospinning method. The sol-gel method with  $\text{CuCrO}_2$  precursor used for the film preparation is illustrated in Figure 1. Chromium acetate ( $(\text{CH}_3\text{CO}_2)_7\text{Cr}_3(\text{OH})_2$ ) and cupric nitrate ( $\text{Cu}(\text{NO}_3)_2 \cdot 3\text{H}_2\text{O}$ ) were combined with a molar ratio of 3:1, and the prepared composition was dissolved in ethanol ( $\text{CH}_3\text{CH}_2\text{OH}$ ) to obtain 0.2 M of the metal source solution. At the same time, polyvinyl pyrrolidone (PVP) ( $(\text{C}_6\text{H}_9\text{NO})_n$ , average MW:1,300,000) (1.5 g) and ethanol (8.5 mL) were applied to the metal source solution (10 mL) to form the main precursor. After effective stirring at 80 °C for 12 h, a sticky gel-like solution of  $\text{CuCrO}_2$ /PVP precursor was achieved. The reaction precursor was put in a 5 mL syringe for the electrospinning process. The syringe was then clamped to a ring stand 5 cm above a stainless steel mesh that was grounded and bowl-shaped. A high-voltage power was attached to the precursor syringe's metal needle, which was linked to the syringe pump. The applied voltage was 16 kV, and the electrospinning precursor feeding rate was 0.12 mL/h. Anisotropic films were prepared using the high-speed spinning collector and the glass substrate was anchored on the roller. The  $\text{CuCrO}_2$  nanowires were electro-spun onto the glass substrate for 2.5 h. Every sample was dried in an oven for 12 h at 80 °C after electrospinning. The dried  $\text{CuCrO}_2$  precursor as spun fiber films on glass substrate were annealed in vacuum condition at 600 °C for 10 min to form  $\text{CuCrO}_2$  films.

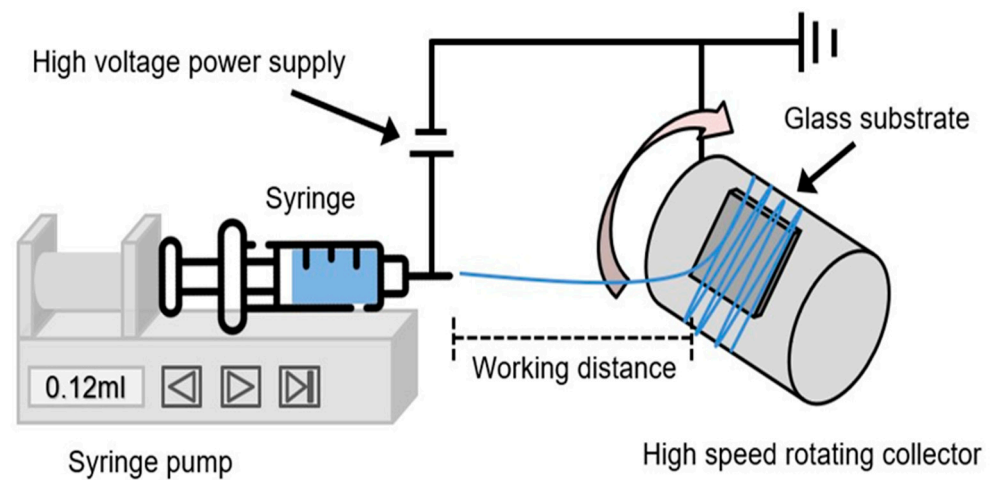


Figure 1. Schematic image of electrospinning experimental setup.

### 3. Results and Discussion

#### 3.1. XRD Analysis of $\text{CuCrO}_2$ Thin Films

The X-ray diffraction analysis (XRD), used to identify the crystal structure of the  $\text{CuCrO}_2$  thin films prepared by electrospinning with 3000 rpm rotating speed on glass substrate after annealing, is shown in Figure 2. The XRD pattern exhibited three main peaks, corresponding to the (006), (012) and (110) planes, which coincided with the typical delafossite structure of  $\text{CuCrO}_2$  (JCPDF Card No. 39-0247). Moreover, based on the XRD pattern study, it was determined that the pure phase of  $\text{CuCrO}_2$  was obtained by annealing at 600 °C for 10 min.

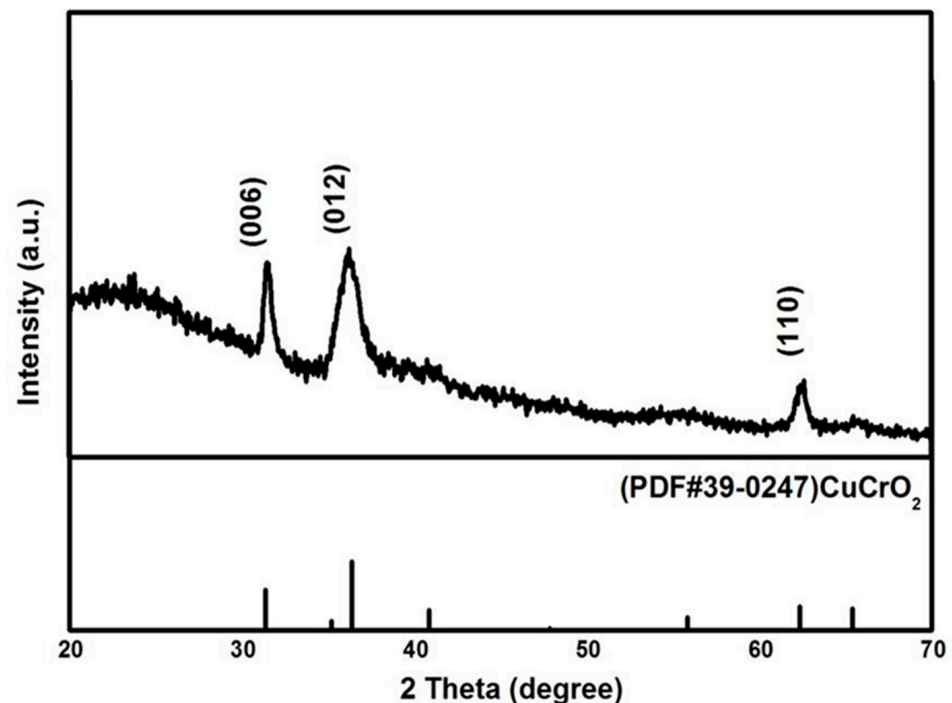
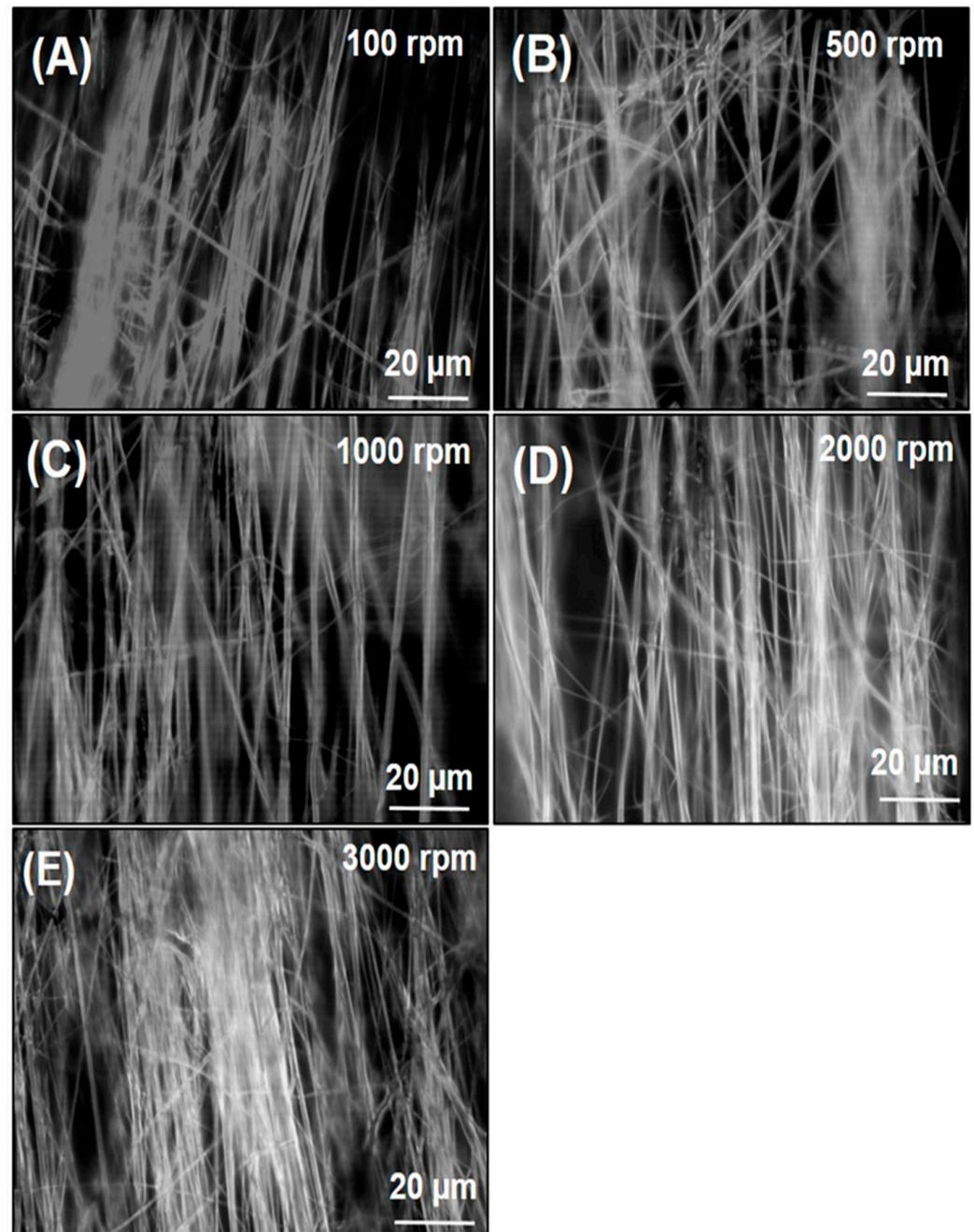


Figure 2. XRD pattern of  $\text{CuCrO}_2$  nanowire deposited by electrospinning at 3000 rpm rotating speed on the glass substrate after annealing at 600 °C.

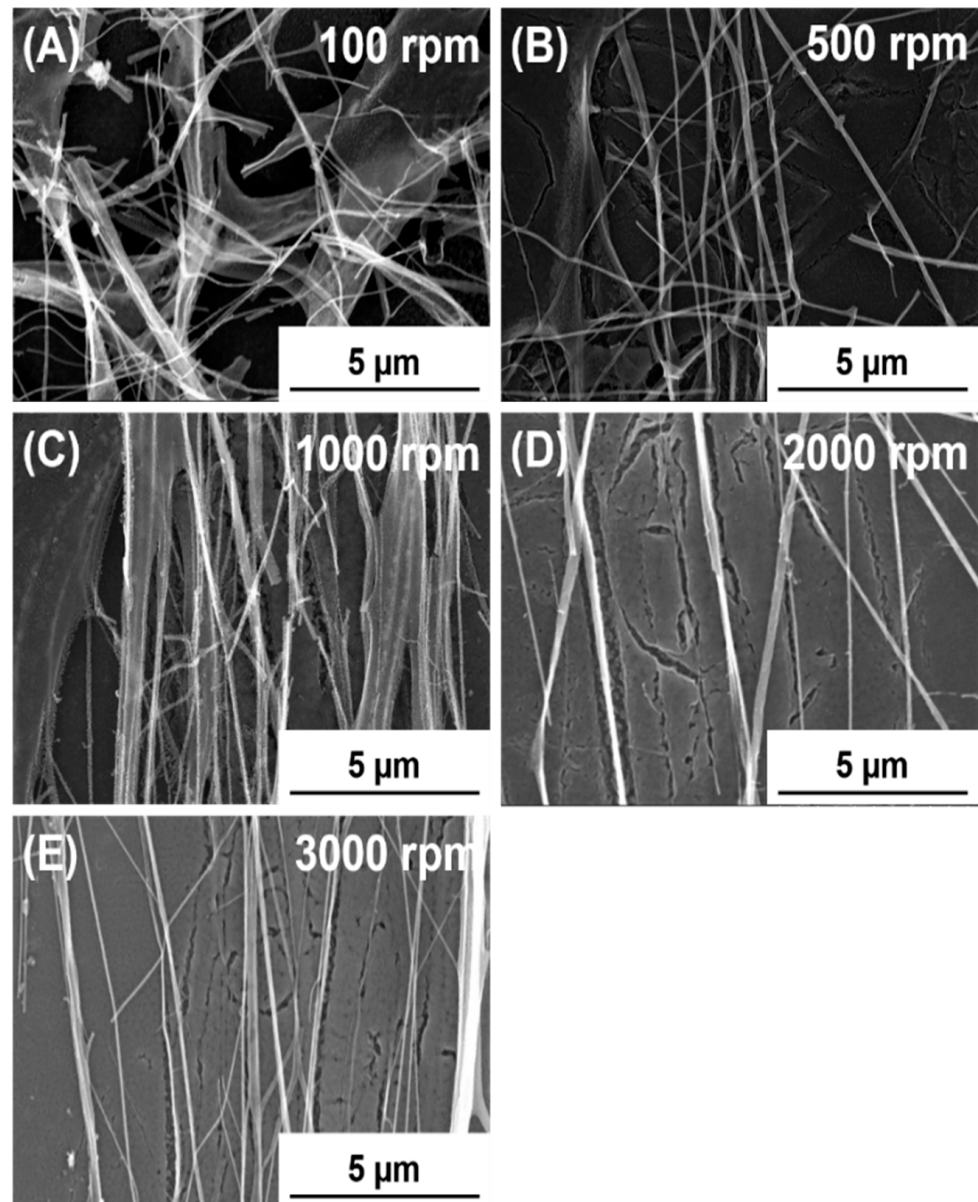
### 3.2. Electron Microscope Studies of Prepared $\text{CuCrO}_2$ Thin Films

Figure 3 presents the optical microscope analysis of  $\text{CuCrO}_2$  thin films deposited on glass substrate at different rotation speeds (100–3000 rpm). As shown in Figure 3A, slow spinning produced disordered nanowires. At a rotation speed of 500 and 1000 rpm, as shown in (Figure 3B,C), the nanowires were still somewhat disordered. At 2000 rpm and above, the nanowire alignment had a more homogeneous direction, as shown in Figure 3D,E.



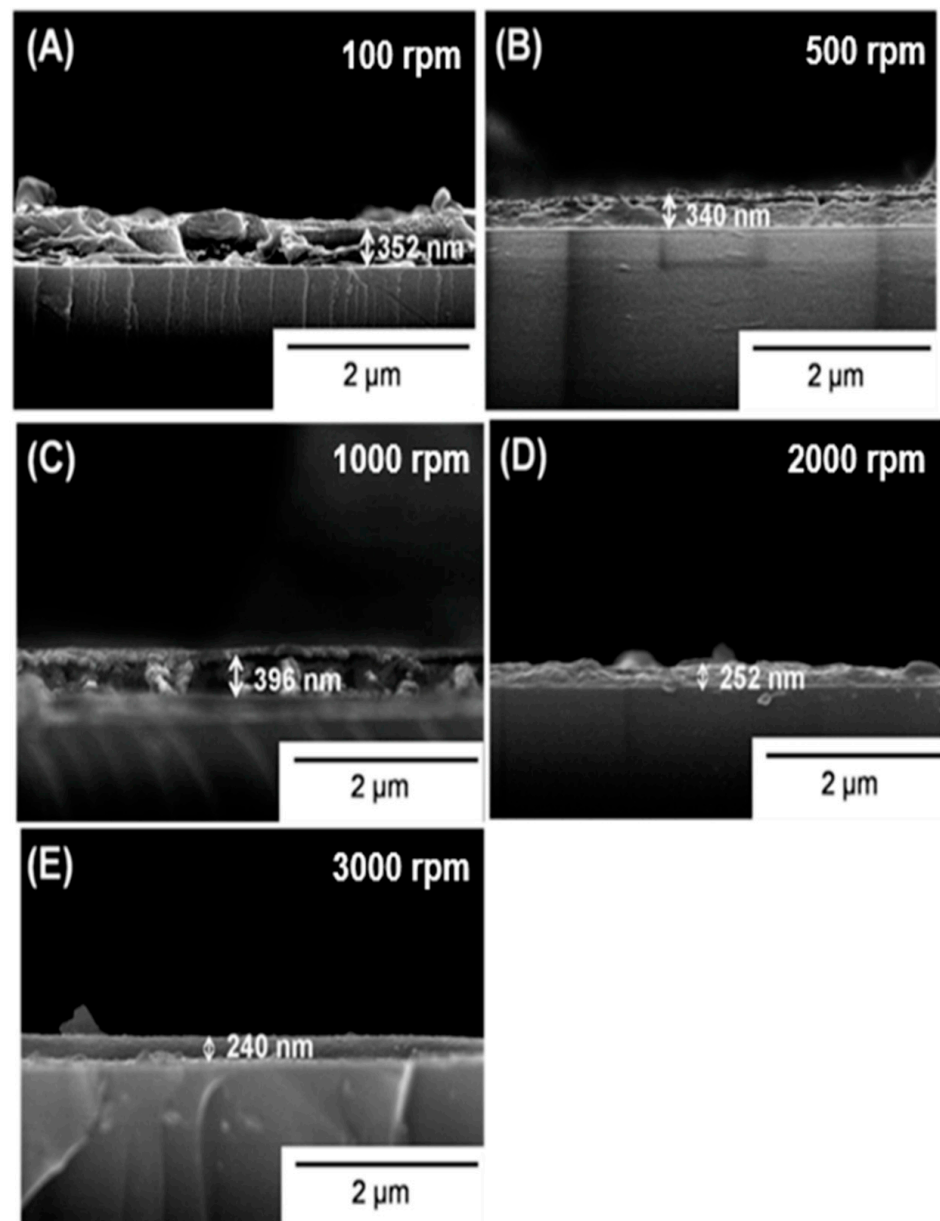
**Figure 3.** Morphology of as-spun precursor nanowires of  $\text{CuCrO}_2$  thin films deposited on glass substrates at different rotating speed and annealed at 600 °C. Speed of rotation: (A) 100 rpm, (B) 500 rpm, (C) 1000 rpm, (D) 2000 rpm, (E) 3000 rpm.

Figure 4 shows FE-SEM analysis of the  $\text{CuCrO}_2$  thin films annealed at  $600\text{ }^\circ\text{C}$  for 10 min in vacuum. The FE-SEM images verified that increasing the rotation speed resulted in better alignment of the nanowires in the depositing direction. The diameters of the nanowires were 112 to 375 nm. Figure 5 presents a cross-sectional FE-SEM image of the  $\text{CuCrO}_2$  nanowires with various rotating speeds from 100 to 3000 rpm. The average thicknesses of the  $\text{CuCrO}_2$  nanowires produced at the different rotation speeds were as follows: (A) 352 nm (100 rpm), (B) 340 nm (500 rpm), (C) 396 nm (1000 rpm), (D) 252 nm (2000 rpm), and (E) 240 nm (3000 rpm).



**Figure 4.** FE-SEM morphology analysis of  $\text{CuCrO}_2$  thin films deposited on glass substrates at different rotating speed and annealed at  $600\text{ }^\circ\text{C}$ . Speed of rotation: (A) 100 rpm, (B) 500 rpm, (C) 1000 rpm, (D) 2000 rpm, (E) 3000 rpm.

The  $\text{CuCrO}_2$  structure on glass substrate was identified by TEM. The TEM samples were processed with a focused ion beam (FIB) with a Pt protective coating. The samples were then cut in directions vertical and parallel to the spinning direction. Figure 6A,B and Figure 7A,B present TEM images of the  $\text{CuCrO}_2$  thin films prepared by electrospinning with a rotating speed of 3000 rpm cut in the two directions. The parallel-direction TEM image clearly shows that the films were well attached to the AZO, and the vertical-direction TEM image exhibits that the films were deposited in layers on the AZO. The EDX analysis in Figures 6C and 7C presents the mapping regions corresponding to (D) Cu, (E) Cr, (F) Al and (G) Zn elements. All results confirmed that the anisotropic  $\text{CuCrO}_2$  thin films were successfully prepared on the AZO by electrospinning.



**Figure 5.** Cross-section FE-SEM of  $\text{CuCrO}_2$  thin films deposited on glass substrates at different rotating speed and annealed at 600 °C for 10 min. Speed of rotation: (A) 100 rpm, (B) 500 rpm, (C) 1000 rpm, (D) 2000 rpm, (E) 3000 rpm.

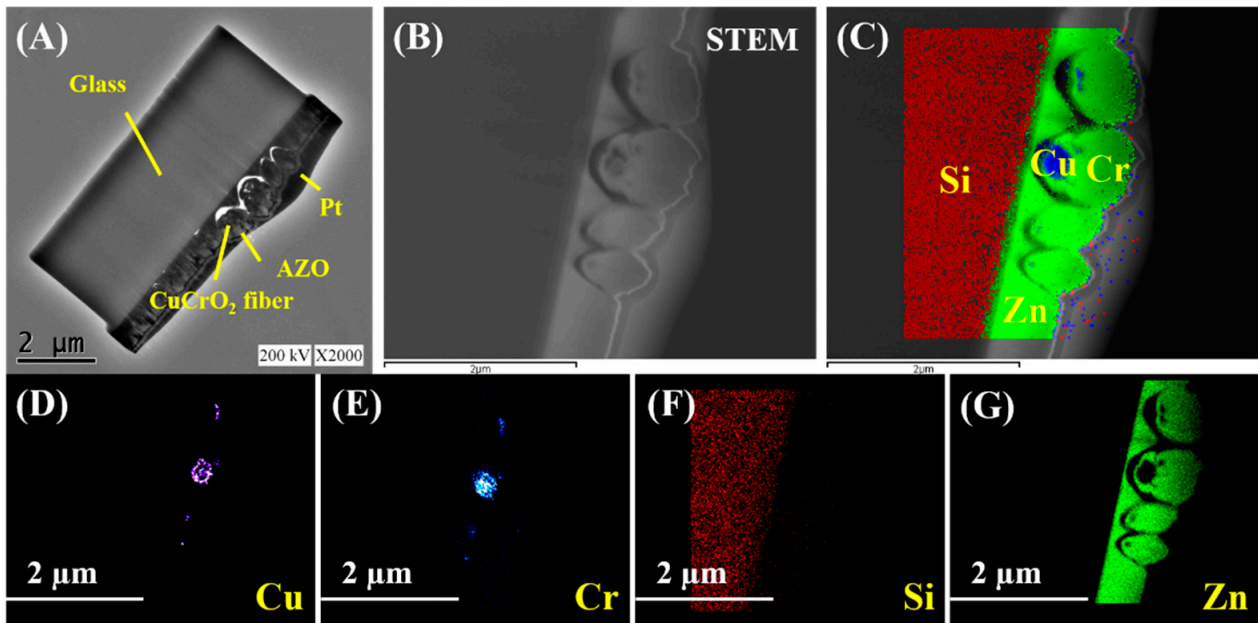


**Figure 6.** (A) TEM, (B) STEM, (C) Mix and EDX-mapping of the parallel direction of the electro-spun  $\text{CuCrO}_2$  thin film prepared at rotating speed of 3000 rpm, (D) Cu, (E) Cr, (F) Al, (G) Zn.

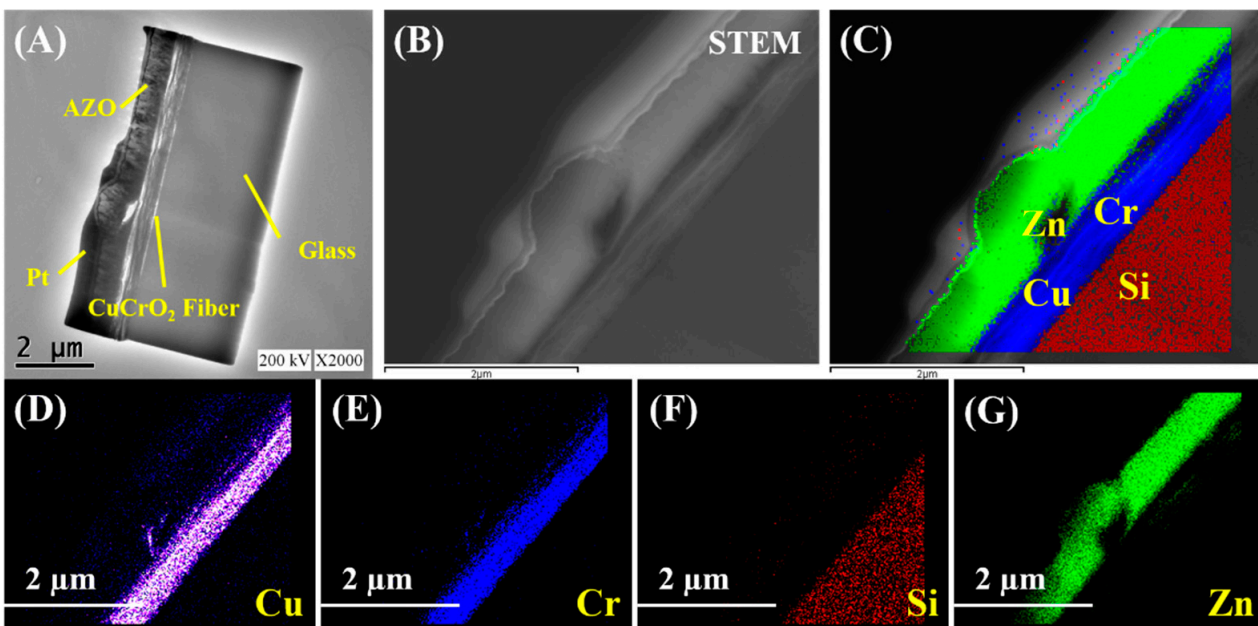


**Figure 7.** (A) TEM, (B) STEM, (C) Mix and EDX-mapping of the vertical direction of the electro-spun  $\text{CuCrO}_2$  thin film by rotating speed of 3000 rpm, (D) Cu, (E) Cr, (F) Si, (G) Zn.

#### 4. Optoelectrical Properties of Dela-fossite-Type $\text{CuCrO}_2$ Thin Films

##### 4.1. Optical Properties

The  $\text{CuCrO}_2$  thin film optical transmission spectrum was examined at wavelengths of 220–1100 nm. Figure 8 displays the optical transmittance spectrum of  $\text{CuCrO}_2$  thin films prepared with various rotating speeds from 100 to 3000 rpm and annealed in vacuum at 600 °C for 10 min. The transmittances of the samples were 55.8% (100 rpm), 69.6% (500 rpm), 75.2% (1000 rpm), 82.1% (2000 rpm), and 81.0% (3000 rpm) in the visible region. The diffusion transmittances of the films were 9.34% (100 rpm), 10.47% (500 rpm), 9.33% (1000 rpm), 8.13% (2000 rpm), and 4.15% (3000 rpm) in the visible region, respectively (Figure 9). We calculate the transmittance haze with Equation (1) after calculating the diffusion transmittances and total transmittances.

$$\text{Transmittance Haze} = D\text{-iffuse transmittance}/\text{Total transmittance} \quad (1)$$

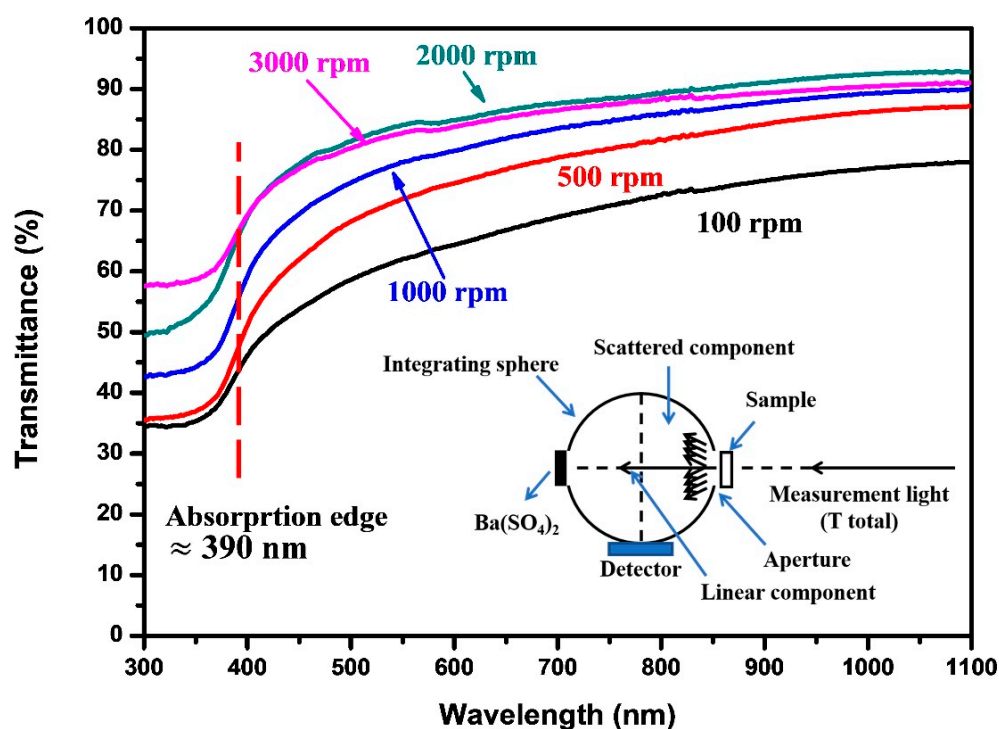


**Figure 8.** UV-Visible transmittance spectra of  $\text{CuCrO}_2$  thin films annealed at 600 °C at different rotating speeds from 100 to 3000 rpm.

Table 1 shows the transmittance haze results of the  $\text{CuCrO}_2$  thin films prepared with various rotating speeds from 100 to 3000 rpm. The results were 16.7% (100 rpm), 15.0% (500 rpm), 12.4% (1000 rpm), 9.9% (2000 rpm), and 5.1% (3000 rpm), respectively. Figure 10 presents the diffusion reflection spectra of the  $\text{CuCrO}_2$  thin films at different rotating speeds. The diffusion reflections were 18.5% (100 rpm), 11.2% (500 rpm), 14.2% (1000 rpm), 11.2% (2000 rpm), and 11.7% (3000 rpm) in the visible region, respectively. We determined the absorption with Equation (2) from the transmittance, diffusion transmittances, and diffusion reflections.

$$A = 1 - (TD + TS + DR + SR) \quad (2)$$

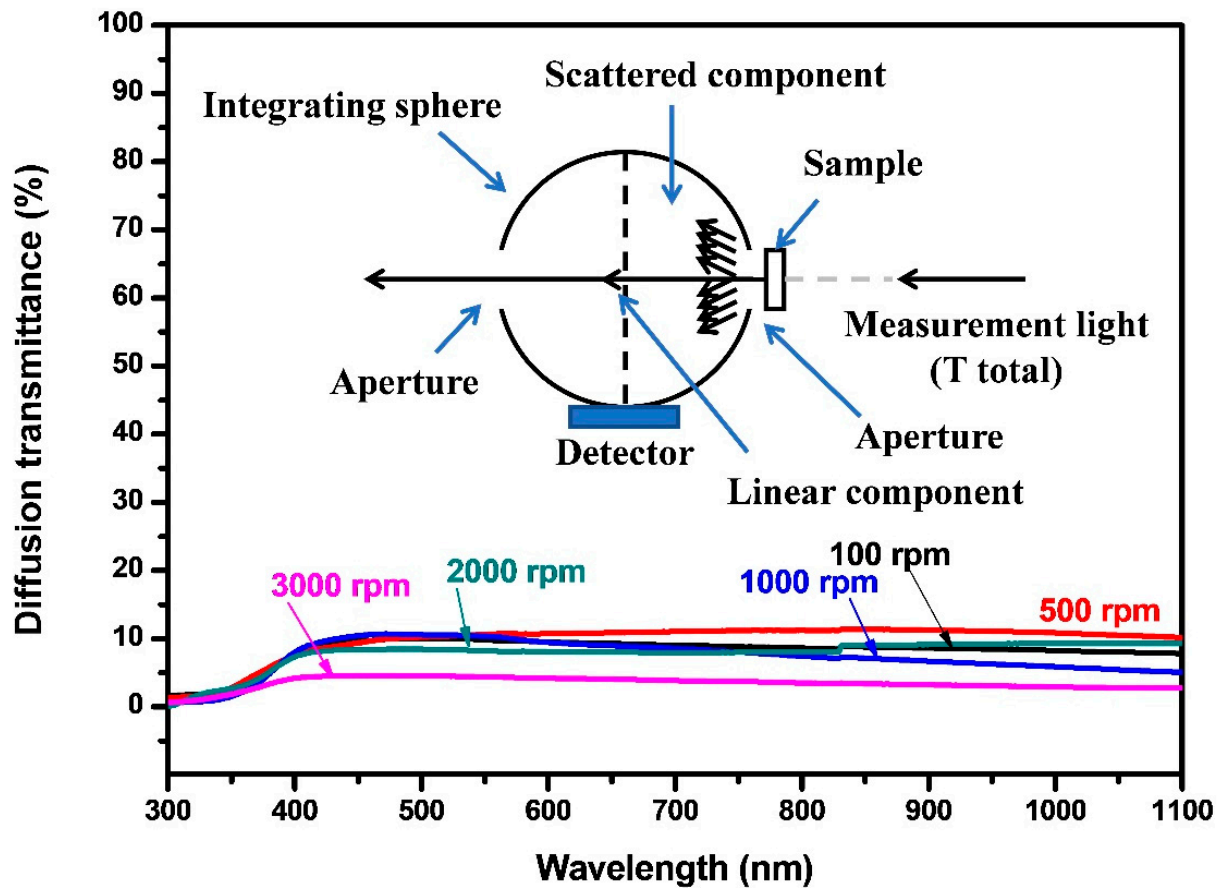


**Figure 9.** UV-Visible diffusion transmittance spectra of CuCrO<sub>2</sub> thin films prepared at different rotating speeds from 100 to 3000 rpm and annealed at 600 °C.

**Table 1.** UV-Visible transmittance haze of CuCrO<sub>2</sub> thin films annealed in vacuum at 600 °C for 10 min in different rotating speed from 100 to 3000 rpm.

Rotation Speed	Haze (%)
100 rpm	16.7%
500 rpm	15%
1000 rpm	12.4%
2000 rpm	9.9%
3000 rpm	5.1%

The absorbance values were 16.36% (100 rpm), 8.73% (500 rpm), 2.27% (1000 rpm), 1.68% (2000 rpm), and 3.15% (3000 rpm). Table 2 lists all the values of total transmittance. To evaluate the optical bandgap and absorption, which corresponds to the electron excitation, the valence band to the conduction band was used. For simple parabolic bands and direct transitions mentioned in Equation (3)

$$\alpha(\nu)n_0h\nu \approx (h\nu - E_g)^n \tag{3}$$

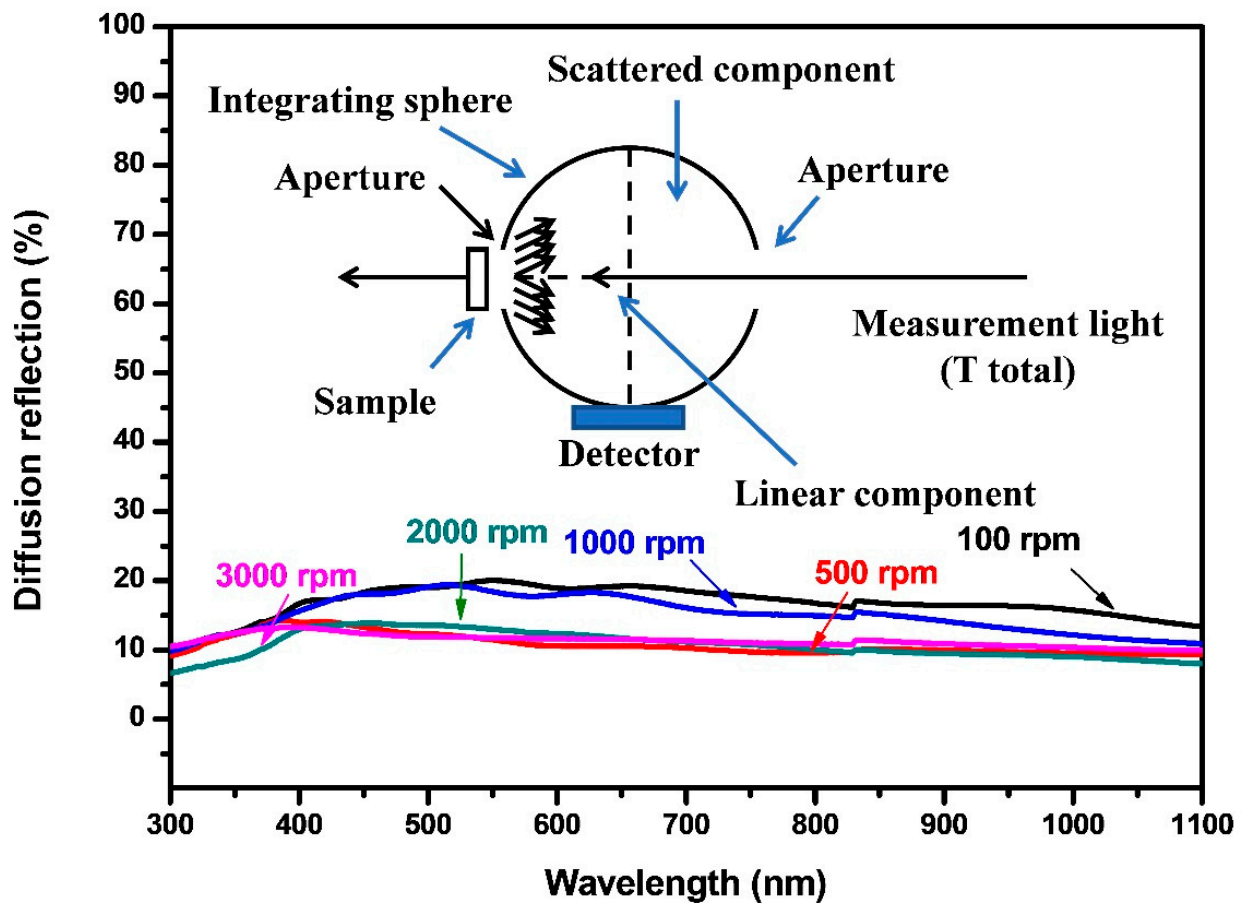


**Figure 10.** UV-Visible diffusion reflection spectra of  $\text{CuCrO}_2$  thin films prepared at different rotating speeds from 100 to 3000 rpm and annealed at 600 °C.

**Table 2.** Detailed values (transmittance, diffusion, reflection, and absorbance) of  $\text{CuCrO}_2$  thin films prepared at different rotating speeds from 100 to 3000 rpm.

T Total (%)	100 rpm	500 rpm	1000 rpm	2000 rpm	3000 rpm
Transmittance	55.8%	69.6%	75.2%	82.1%	81.0%
Diffusion	9.34%	10.47%	8.33%	5.02%	4.15%
Reflection	18.5%	11.2%	14.2%	11.2%	11.7%
Absorb	16.36%	8.73%	2.27%	1.68%	3.15%

In the quantum-mechanical sense, where  $n$  is a constant of  $1/2$  for permitted transitions and  $3/2$  for prohibited transitions:  $n_0$  is the refractive index,  $h\nu$  is the photon energy, and  $E_g$  is the bandgap energy of the material under investigation [24]. According to the absorption edge of  $\text{CuCrO}_2$  thin films prepared with different rotating speed from 100 to 3000 rpm, all of the  $\text{CuCrO}_2$  thin films absorption edge fixed at 390 nm wavelength which could preliminary estimate the material energy band gap. Based on Equation (4), the band gaps of  $\text{CuCrO}_2$  thin films were estimated at 3.17 eV, respectively [36–39]. Figure 11 reveals the Tuac Plot of the  $\text{CuCrO}_2$  thin films prepared at different rotating speeds from 100 to 3000 rpm. However, the band gaps of  $\text{CuCrO}_2$  thin films determined by Tuac Plot were estimated at 3.0 eV approximate.

$$E(\text{eV}) = hc/\lambda = 1240/\lambda (\text{nm}) \quad (4)$$

#### 4.2. Electrical Properties

Figure 12 indicates the resistivity measured by the system of the two-point probe. The resistivity of  $\text{CuCrO}_2$  thin films produced at different speeds of rotation and vacuum-recovered at  $600\text{ }^\circ\text{C}$  for 10 min is shown in Table 3. The values of parallel resistivity were  $6.79 \times 10^7$  (100 rpm),  $2.12 \times 10^7$  (500 rpm),  $1.68 \times 10^6$  (1000 rpm),  $4.21 \times 10^6$  (2000 rpm), and  $1.88 \times 10^5$  (3000 rpm), respectively. Those of vertical resistivity were  $4.88 \times 10^7$  (100 rpm),  $1.05 \times 10^6$  (500 rpm),  $7.73 \times 10^6$  (1000 rpm),  $2.67 \times 10^9$  (2000 rpm), and  $6.03 \times 10^7$  (3000 rpm), respectively. The anisotropic  $\text{CuCrO}_2$  thin film conductivities in the parallel and vertical directions differed by nearly two to three orders of magnitude. The differences for the rotation speeds of 2000 and 3000 rpm were especially obvious.

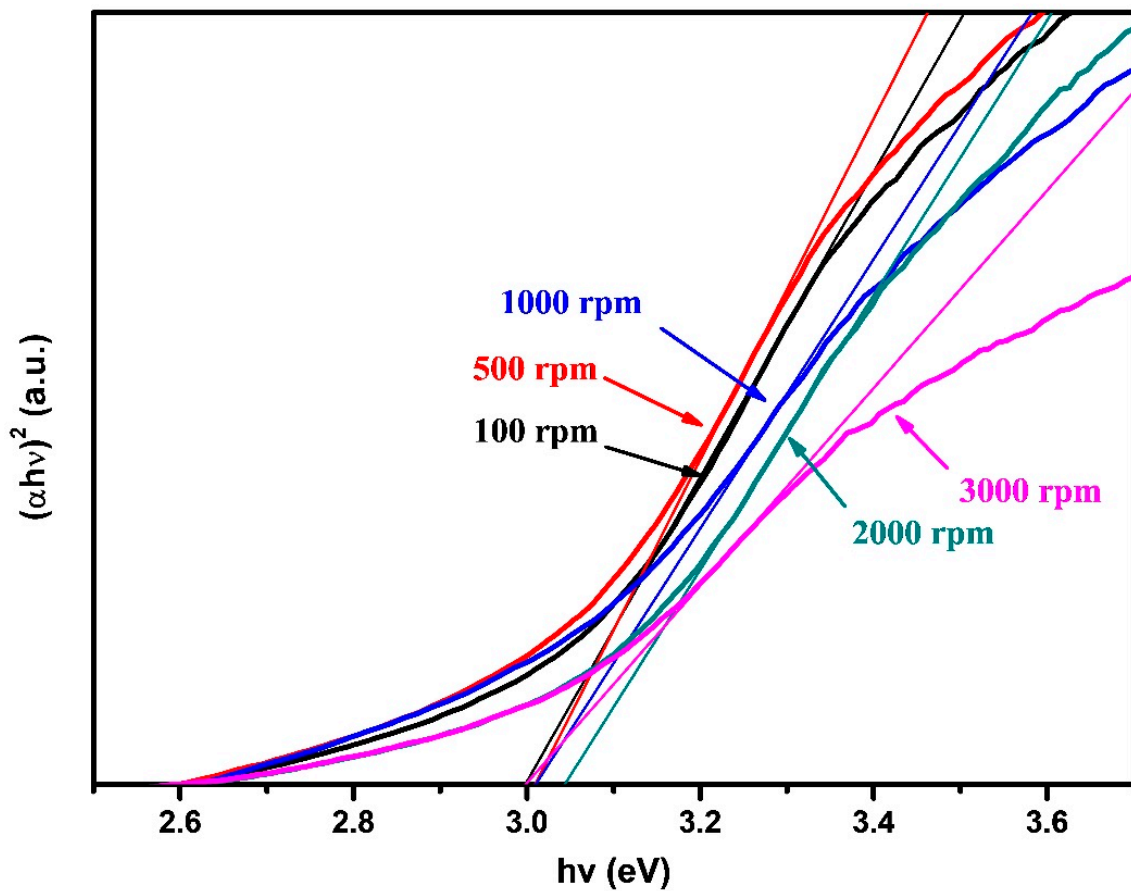


**Figure 11.** Tuac Plot and estimated energy band gaps of  $\text{CuCrO}_2$  thin films prepared at different rotating speeds from 100 to 3000 rpm and annealed at  $600\text{ }^\circ\text{C}$ .

**Table 3.** Detailed electrical resistance values of  $\text{CuCrO}_2$  thin films prepared at different rotating speeds from 100 to 3000 rpm and annealed at  $600\text{ }^\circ\text{C}$ .

Rotation Speed	Resistivity ( $\Omega$ ) Parallel	Resistivity ( $\Omega$ ) Vertical	Resistivity Ratio Vertical/Parallel
100 rpm	$6.79 \times 10^7$	$4.88 \times 10^7$	0.71
500 rpm	$2.12 \times 10^6$	$1.05 \times 10^6$	0.49
1000 rpm	$1.68 \times 10^6$	$7.73 \times 10^6$	4.60
2000 rpm	$4.21 \times 10^6$	$2.67 \times 10^9$	634.20
3000 rpm	$1.88 \times 10^5$	$6.03 \times 10^7$	320.74

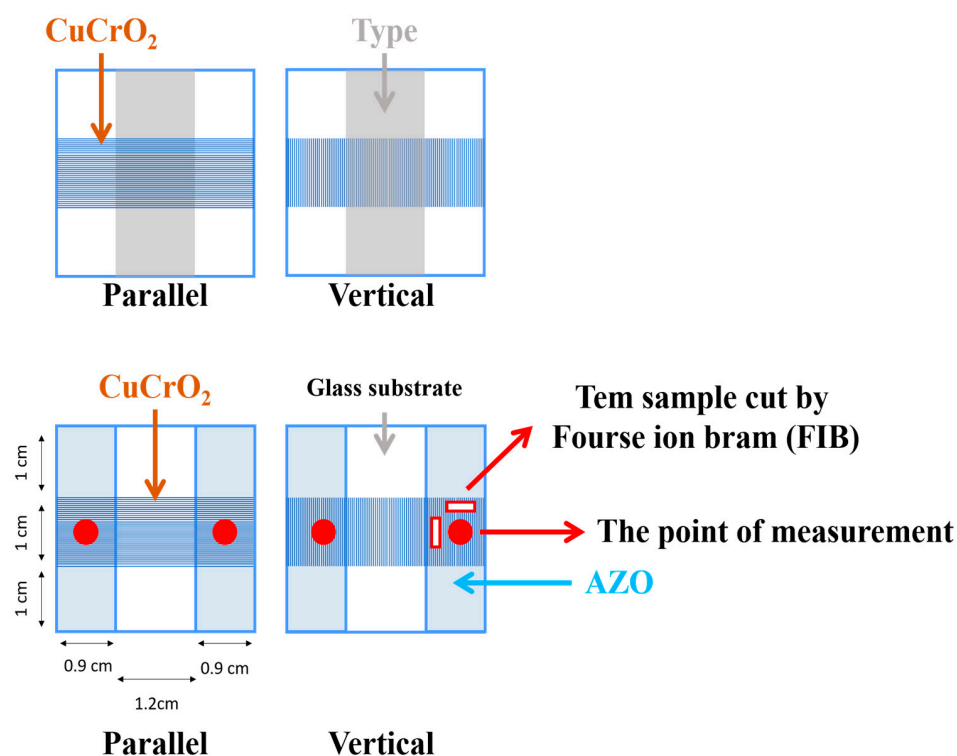


**Figure 12.** Schematic diagram of the resistivity in the vertical and parallel directions of  $\text{CuCrO}_2$  thin films annealed at  $600\text{ }^\circ\text{C}$  at different rotating speeds from 100 to 3000 rpm measured by FIB.

## 5. Conclusions

In this study, anisotropic  $\text{CuCrO}_2$  thin films were successfully fabricated by electrospinning on glass substrate. The XRD patterns suggested that the pure phase of the  $\text{CuCrO}_2$  thin film was achieved by annealing in vacuum at  $600\text{ }^\circ\text{C}$  for 10 min. SEM revealed that higher rotation speeds resulted in better alignment of the nanowires, leading to better morphology of the  $\text{CuCrO}_2$  thin films. Moreover, higher rotation speeds also produced films with higher transmittance values. The transmittances for the different rotation speeds were 55.8% (100 rpm), 69.6% (500 rpm), 75.2% (1000 rpm), 82.1% (2000 rpm), and 81.0% (3000 rpm) in the visible region, respectively. The haze results were 16.7% (100 rpm), 15.0% (500 rpm), 12.4% (1000 rpm), 9.9% (2000 rpm), and 5.1% (3000 rpm) in the visible region, respectively. The parallel and vertical electrical conductivities of the anisotropic  $\text{CuCrO}_2$  thin films generated at 2000 rpm and 3000 rpm had differences of nearly two to three magnitude orders. In addition, higher rotation speeds yielded  $\text{CuCrO}_2$  thin films with higher optical transmittance.

**Author Contributions:** Conceptualization, Writing—original draft, Investigation, C.-L.Y.; C.-H.W.; Visualization, Investigation, Software, R.-J.H.; Writing—original draft, S.S.; Validation. Supervision, Methodology, T.-W.C.; Writing & editing, C.D. All authors have read and agreed to the published version of the manuscript.

**Funding:** This research was funded by the Ministry of Science and Technology of Taiwan (MOST 108-2221-E-027-056, MOST 109-2221-E-027-068-, MOST 109-2222-E-027-001- and MOST 109-2221-E-027-059-) and the National Taipei University of Technology-University of Science and Technology Beijing Joint Research Program (NTUT-USTB-105-7). The authors are grateful to the Precision Research and Analysis Centre of the National Taipei University of Technology (NTUT) for providing the measurement facilities.

**Institutional Review Board Statement:** Not applicable.

**Informed Consent Statement:** Not applicable.

**Data Availability Statement:** Data is contained within the article.

**Conflicts of Interest:** The authors declare no conflict of interest.

## References

1. Stadler, A. Transparent conducting oxides—An up-to-date overview. *Materials* **2012**, *5*, 661–683. [[CrossRef](#)]
2. Castaneda, L. Present status of the development and application of transparent conductors oxide thin solid films. *Mater. Sci. Appl.* **2011**, *2*, 1233–1242. [[CrossRef](#)]
3. Wei, R.; Tang, X.; Hu, L.; Yang, J.; Zhu, X.; Song, W.; Dai, J.; Zhu, X.; Sun, Y. Facile chemical solution synthesis of p-type delafossite Ag-based transparent conducting AgCrO<sub>2</sub> films in an open condition. *J. Mater. Chem. C* **2017**, *5*, 1885–1892. [[CrossRef](#)]
4. Minami, T. Transparent conducting oxide semiconductors for transparent electrodes. *Semicond. Sci. Technol.* **2005**, *20*, S35–S44. [[CrossRef](#)]
5. Wager, J.F. Transparent electronics. *Science* **2003**, *300*, 1245–1246. [[CrossRef](#)]
6. Granqvist, C.G. Transparent conductors as solar energy materials: A panoramic review. *Sol. Energy Mater. Sol. Cells* **2007**, *91*, 1529–1598.
7. Nomura, K.; Ohta, H.; Ueda, K.; Kamiya, T.; Hirano, M.; Hosono, H. Thin-film transistor fabricated in single-crystalline transparent oxide semiconductor. *Science* **2003**, *300*, 1269–1272. [[CrossRef](#)]
8. Wang, Z.; Nayak, P.K.; Frescas, J.A.C.; Alshareef, H.N. Recent Developments in p-Type Oxide Semiconductor Materials and Devices. *Adv. Mater.* **2016**, *28*, 3831–3892. [[CrossRef](#)]
9. Kawazoe, H.; Yasukawa, M.; Hyodo, H.; Kurita, M.; Yanagi, H.; Hosono, H. P-Type Electrical Conduction in Transparent Thin Films of CuAlO<sub>2</sub>. *Nature* **1997**, *389*, 939–942. [[CrossRef](#)]
10. Wu, S.; Deng, Z.; Dong, W.; Shao, J.; Fang, X. Effect of deposition atmosphere on the structure and properties of Mg doped CuCrO<sub>2</sub> thin films prepared by direct current magnetron sputtering. *Thin Solid Films* **2015**, *595*, 124–128. [[CrossRef](#)]
11. Thahab, S.M.; Alkhayatt, A.H.O.; Zgair, I.A. Influences of post-annealing temperature on the structural and electrical properties of mixed oxides (CuFeO<sub>2</sub> and CuFe<sub>2</sub>O<sub>4</sub>) thin films prepared by spray pyrolysis technique. *Mater. Sci. Semicond. Process.* **2016**, *41*, 436–440. [[CrossRef](#)]
12. Shimode, M.; Sasaki, M.; Mukaida, K. Synthesis of the delafossite-type CuInO<sub>2</sub>. *J. Solid State Chem.* **2000**, *151*, 16–20. [[CrossRef](#)]
13. Tambunan, O.T.; Tukiman, H.; Parwanta, K.J.; Jeong, D.W.; Jung, C.U.; Rhee, S.J.; Liu, C. Structural and optical properties of SrCu<sub>2</sub>O<sub>2</sub> films deposited on sapphire substrates by pulsed laser deposition. *Superlattices Microstruct.* **2012**, *52*, 774–781. [[CrossRef](#)]
14. Nagarajan, R.; Draeseke, A.D.; Sleight, A.W.; Tate, J. P-Type Conductivity in CuCr<sub>1-x</sub>Mg<sub>x</sub>O<sub>2</sub> Films and Powders. *J. Appl. Phys.* **2001**, *89*, 8022. [[CrossRef](#)]
15. Barnabe, A.; Thimont, Y.; Lalanne, M.; Presmanes, L.; Tailhades, P. P-Type conducting transparent characteristics of delafossite Mg-doped CuCrO<sub>2</sub> thin films prepared by RF-sputtering. *J. Mater. Chem. C* **2015**, *3*, 6012–6024. [[CrossRef](#)]
16. Osullivan, M.; Stamenov, P.; Alaria, J.; Venkatesan, M.; Coey, J.M.D. Magnetoresistance of CuCrO<sub>2</sub> based delafossite films. *J. Phys. Conf. Ser.* **2010**, *200*, 052021. [[CrossRef](#)]
17. Kim, S.Y.; Lee, J.H.; Kim, J.J.; Heo, Y.W. Preferential growth orientations of CuCrO<sub>2</sub> films grown by pulsed laser deposition. *Curr. Appl. Phys.* **2012**, *12*, 123–126. [[CrossRef](#)]
18. Mahapatra, S.; Shivashankar, S.A. Low-pressure metal-organic CVD of transparent and p-type conducting CuCrO<sub>2</sub> thin films with high conductivity. *Chem. Vap. Depos.* **2003**, *9*, 238–240. [[CrossRef](#)]
19. Chiu, T.W.; Tonooka, K.; Kikuchi, N. Influence of oxygen pressure on the structural, electrical and optical properties of VO<sub>2</sub> thin films deposited on ZnO/glass substrates by pulsed laser deposition. *Thin Solid Films* **2010**, *518*, 7441–7444. [[CrossRef](#)]
20. Chiu, T.W.; Tonooka, K.; Kikuchi, N. Fabrication of transparent CuCrO<sub>2</sub>: Mg/ ZnO p-n junctions prepared by pulsed laser deposition on glass substrate. *Vacuum* **2008**, *83*, 614–617. [[CrossRef](#)]
21. Chiu, T.W.; Tonooka, K.; Kikuchi, N. Fabrication of ZnO and CuCrO<sub>2</sub>: Mg thin films by pulsed laser deposition with in situ laser annealing and its application to oxide diodes. *Thin Solid Films* **2008**, *516*, 5941–5947. [[CrossRef](#)]
22. Chen, H.Y.; Yang, C.C. Transparent p-type Zn-doped CuCrO<sub>2</sub> films by sol-gel processing. *Surf. Coat. Technol.* **2013**, *231*, 277–280. [[CrossRef](#)]
23. Chiu, T.W.; Chen, Y.A.; Lee, H.C.; Hong, S.Z. Preparing and applying nanosheets in controlling the orientation of TiO<sub>2</sub> thin films. *Ceram. Int.* **2015**, *41*, S213–S217. [[CrossRef](#)]
24. Zhou, S.; Fang, X.; Deng, Z.; Li, D.; Dong, W.; Tao, R.; Meng, G.; Wang, T.; Zhu, X. Hydrothermal synthesis and characterization of CuCrO<sub>2</sub> laminar nanocrystals. *J. Cryst. Growth* **2008**, *310*, 5375–5379. [[CrossRef](#)]
25. Kim, D.S.; Park, S.J.; Jeong, E.K.; Lee, H.K.; Choi, S.Y. Optical and electrical properties of p-type transparent conducting CuAlO<sub>2</sub> thin film. *Thin Solid Films* **2007**, *515*, 5103–5108. [[CrossRef](#)]
26. Tsuboi, N.; Moriya, T.; Kobayashi, S.; Shimizu, H.; Kato, K.; Kaneko, F. Characterization of CuAlO<sub>2</sub> thin films prepared on sapphire substrates by reactive sputtering and annealing. *Jpn. J. Appl. Phys.* **2008**, *47*, 592–595. [[CrossRef](#)]
27. Chiu, T.W.; Yang, Y.C.; Yeh, A.C.; Wang, Y.P.; Feng, Y.W. Antibacterial property of CuCrO<sub>2</sub> thin films prepared by RF magnetron sputtering deposition. *Vacuum* **2013**, *87*, 174–177. [[CrossRef](#)]
28. Yang, T.C.K.; Yang, Y.L.; Juang, R.C.; TWChiu Chen, C.C. The novel preparation method of high-performance thermochromic vanadium dioxide thin films by thermal oxidation of vanadium-stainless steel co-sputtered films. *Vacuum* **2015**, *121*, 310–316. [[CrossRef](#)]

29. Bhardwaj, N.; Kundu, S.C. Electrospinning: A fascinating fiber fabrication technique. *Biotechnol. Adv.* **2010**, *28*, 325–347. [[CrossRef](#)]
30. Chiu, T.W.; Chen, Y.T. Preparation of CuCrO<sub>2</sub> nanowires by electrospinning. *Ceram. Int.* **2015**, *41*, S407–S413. [[CrossRef](#)]
31. Liang, D.; Hsiao, B.S.; Chu, B. Functional electrospun nanofibrous scaffolds for biomedical applications. *Adv. Drug Deliv. Rev.* **2007**, *59*, 1392–1412. [[CrossRef](#)]
32. Sill, T.J.; Von Recum, H.A. Electrospinning: Applications in drug delivery and tissue engineering. *Biomaterials* **2008**, *29*, 1989–2006. [[CrossRef](#)]
33. Doshi, J.; Reneker, D.H. Electrospinning process and applications of electrospun fibers. *Conf. Rec. IAS Annu. Meet.* **1993**, *3*, 1698–1703.
34. Yarin, A.L.; Koombhongse, S.; Reneker, D.H. Bending instability in electrospinning of nanofibers. *J. Appl. Phys.* **2001**, *89*, 3018–3026. [[CrossRef](#)]
35. Adomaviciute, E.; Milasius, R. The Influence of Applied Voltage on Poly(vinyl alcohol) (PVA) Nanofibre Diameter. *Fibres Text. East. Eur.* **2007**, *5*, 69–72.
36. Sadik, P.W.; Ivill, M.; Craciun, V.; Norton, D.P. Electrical transport and structural study of CuCr<sub>1-x</sub>Mg<sub>x</sub>O<sub>2</sub> delafossite thin films grown by pulsed laser deposition. *Thin Solid Films* **2009**, *517*, 3211–3215. [[CrossRef](#)]
37. Li, D.; Fang, X.D.; Deng, Z.H.; Dong, W.W.; Tao, R.H.; Zhou, S.; Wang, J.M.; Wang, T.; Zhao, Y.P.; Zhu, X.B. Electronic transition and electrical transport properties of delafossite CuCr<sub>1-x</sub>Mg<sub>x</sub>O<sub>2</sub> (0 ≤ x ≤ 12%) films prepared by the sol-gel method: A composition dependence study. *J. Alloys Compd.* **2009**, *486*, 462. [[CrossRef](#)]
38. Wang, Y.F.; Gu, Y.J.; Wang, T.; Shi, W.Z. Magnetic, optical and electrical properties of Mn-doped CuCrO<sub>2</sub> thin films prepared by chemical solution deposition method. *J. Sol-Gel Sci. Technol.* **2011**, *59*, 222–227. [[CrossRef](#)]
39. Chiu, T.W.; Shih, J.H.; Chang, C.H. Preparation and properties of CuCr<sub>1-x</sub>Fe<sub>x</sub>O<sub>2</sub> thin films prepared by chemical solution deposition with two-step annealing. *Thin Solid Films* **2016**, *618*, 151–158. [[CrossRef](#)]